International Journal of Machine Tools & Manufacture 50 (2010) 538–551

Contents lists available at ScienceDirect

International Journal of Machine Tools & Manufacture

journal homepage: www.elsevier.com/locate/ijmactool

A closed form mechanistic cutting force model for helical peripheral milling of ductile metallic alloys

Abhijit Bhattacharyya [a,1], John K. Schueller [a,*], Brian P. Mann [b], John C. Ziegert [c], Tony L. Schmitz [a], Fred J. Taylor [d], Norman G. Fitz-Coy [a]

[a] Department of Mechanical & Aerospace Engineering, University of Florida, Gainesville, FL 32611, USA
[b] Department of Mechanical Engineering and Materials Science, Duke University, Durham, NC 27708, USA
[c] Department of Mechanical Engineering, Clemson University, Clemson, SC 29634, USA
[d] Department of Computer and Information Science and Engineering, University of Florida, Gainesville, FL 32611, USA

ARTICLE INFO

Article history:
Received 30 September 2009
Received in revised form
2 March 2010
Accepted 8 March 2010
Available online 15 March 2010

Keywords:
Cutting force
Cutting coefficients
Helical milling
Analytical model
Runout
Uncertainty

ABSTRACT

A closed form mechanistic model is developed for cutting forces in helical peripheral milling (endmilling) of ductile metallic alloys. This paper presents an alternative derivation, using the frontal chip area, to describe two series of cutting force expressions—one using a Heaviside unit step function and the other using a Fourier series expansion. A specific advantage of the present work is highlighted by deriving analytical expressions for sensitivity coefficients required to analytically propagate the uncertainty in the cutting-force model parameters. Another advantage is that even very small radial immersions can be used to derive cutting coefficients reliably, along with their variances. The aforementioned analytical investigations are applied to a series of experimental cutting tests to estimate the force-model cutting coefficients. Experimental investigations include the study of a tool having radial runout. Finally, confidence intervals are placed on predicted forces which experimentally verify the validity of the proposed force model.

1. Introduction

Machining with helical endmills is one of the most widely used processes in the manufacture of prismatic parts. Predictive models of cutting forces in endmilling are required for various purposes including the estimation of power consumed, and the prediction of stability and surface placement. Applications based on real time cutting force sensing, including tool wear and tool breakage monitoring, have the potential to use predictive models.

A mechanistic model presented by Sabberwal [15] related the tangential force to the chip area with the cutting coefficient being the constant of proportionality. The coefficient was called the specific pressure, and was experimentally demonstrated to be independent of the helix angle for a few work materials. In a review paper, Ehman et al. [6] discussed various formulations of cutting force models available in the literature. Tlusty [21] has described the milling process in great detail, including the modeling of cutting forces. Tlusty and MacNeil [22] were the first to present a closed form analytical solution for two components of the force, in the plane of cutter rotation, for helical peripheral milling. Four separate sets of equation were used to describe each force component. Altintas and Spence [2] presented another two dimensional solution in which different expressions were used depending on the position of the cutter in one rotation. A two dimensional, Fourier series based solution of Schmitz and Mann [18] includes the effect of the helix angle by dividing the cutter into thin axial disks and summing the effects to obtain the total force. A three dimensional integral model was developed by Mann et al. [13] using an equivalent complex Fourier series representation of forces to facilitate symbolic manipulation. Abrari and Elbestawi [1] published a three dimensional closed form solution where the forces were expressed as a linear combination of a set of basis functions, but the linearized cutting coefficients were replaced with a matrix which incorporated the helix angle. Engin and Altintas [7] have offered a general solution for a mechanistic model in a set of integral expressions. The integrations have to be carried out by the user for any specific endmilling process.

The three dimensional force model presented in this paper differs from prior work in several ways. Each force component has a single, closed form expression which is valid for the entire cutter rotation, but the simple structure of linearized cutting coefficients is retained. Any arbitrary value of radial immersion, and hence very small immersions, can be used to experimentally determine

* Corresponding author.
E-mail addresses: abmech@ufl.edu (A. Bhattacharyya), schuejk@ufl.edu (J.K. Schueller).
[1] Present address: 21 SE 11th Ave, Apt 2, Fort Lauderdale, FL 33301, USA.

0890-6955/$ - see front matter © 2010 Elsevier Ltd. All rights reserved.
doi:10.1016/j.ijmachtools.2010.03.003

the cutting coefficients. A particular feature of the model is that the axial projected chip area is related to the axial force component, unlike the general practice of relating the rake face chip area (Fig. 1). This ensures that the axial force component automatically vanishes as the helix angle goes to zero in a straight fluted cutter. It is not necessary to force the axial cutting coefficient to go to zero for straight fluted cutters.

In mechanistic force models, the experimentally determined coefficients have uncertainties and so do force measurements and cutter runout measurements. When these measured values of coefficients and runout are used as inputs in force prediction, the uncertainties propagate through the model. The uncertainty analysis performed here is the first such attempt in force modeling for helical peripheral milling. The sensitivity analysis, used to track the uncertainty propagation, remains compact because the components of force have single expressions valid for the entire cutter rotation.

Two different versions of the force model are presented. One is based on a step function approach, whereas the other is a Fourier series model. In the Heaviside unit step function based model an exact representation of the force is obtained, and this model is useful for most applications. However, the derivatives of the forces, with respect to the cutter rotation angle, are discontinuous. In a rare application when symbolic expressions for such derivatives may be necessary, the user may prefer the alternative formulation which is based on Fourier trigonometric series. Truncated series sums provide sufficiently accurate forces, and have the advantage that derivatives of the forces, with respect to cutter rotation angle, are continuous.

This paper is organized as follows. First, the basic, idealized model is summarized, which includes the force model, method of experimental cutting coefficient extraction, and the cutting coefficient model for the contributions of a single tooth. Next, the multiple tooth formulation is described including the effects of differential pitch and radial runout. Then the cutting coefficients are experimentally extracted and associated variances are calculated. Uncertainties are then propagated through the model to obtain confidence intervals on the predicted forces. Finally, the force predictions are experimentally verified and the results are discussed.

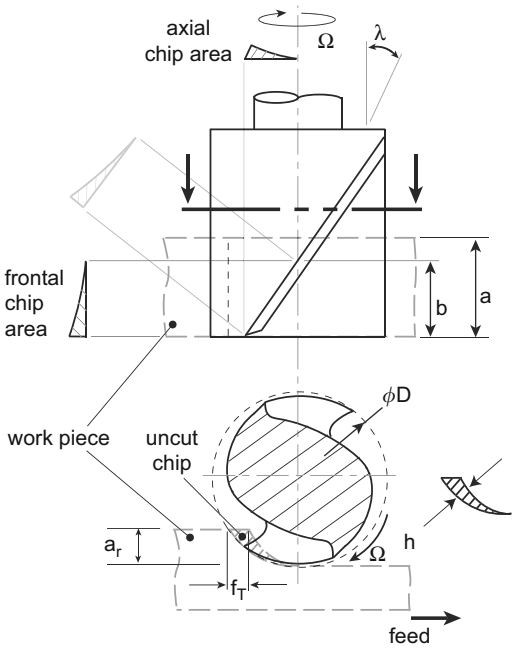

Fig. 1. Terminology: λ = helix angle, D = endmill diameter, a = commanded (nominal) axial depth of cut, a_r = radial depth of cut, f_T = feed per tooth, and Ω = spindle speed. The instantaneous axial depth of cut, b, and the nominal chip thickness, h, vary with cutter rotation. The rake face chip area (gray region, not labeled) is not used in the model. A two fluted, right handed endmill is illustrated in up-milling configuration.

2. Analytical description of chip geometry

This section defines the terminology used to describe a peripheral milling process along with the complexities of obtaining the chip shape for a helical endmill. The aim is to capture the shape and size of the chip as the cutter rotates, since knowledge of the frontal and axial projections of the tool chip interface area can yield the force components after multiplying by the respective cutting coefficients.

The geometry of helical peripheral milling is illustrated in Fig. 1 which shows the helix angle, λ, and the diameter, D, which describe the tool geometry. The commanded (nominal) axial depth of cut, a, the radial depth of cut, a_r, the feed per tooth, f_T, and the spindle speed, Ω, are fixed parameters set by the machinist. The instantaneous axial depth of cut, b, varies with cutter rotation because of the helical flute. Note that b is also the frontal (projected) chip width and, in this paper, b is simply called the chip width. The nominal chip thickness, h, is defined in the plane of cutter rotation, and it is measured in the radial direction. Inspection of Fig. 1 shows that the chip thickness varies as the cutter rotates. The percentage radial immersion, RI is defined as

$$\%RI \triangleq \frac{a_r}{D} \times 100 \tag{1}$$

Cutter-workpiece engagement configurations depend on the relative direction of cutter rotation and the feed direction, combined with the numerical value of the RI. In Fig. 1 the sense of cutter rotation is such that the cutting speed at the entry of the cut is directed opposite to the direction of the feed, and the RI is less than 50%. This results in an up-milling configuration, where the cut begins with zero chip thickness. If the direction of feed were reversed, the resulting configuration would be down-milling, where the cut ends with a zero chip thickness. RI values exceeding 50% result in mixed-mode configurations. The 100% RI results in slotting cuts.

Fig. 1 also illustrates the concept of frontal and axial chip areas. In the force model described here, the frontal chip area is related to the force components in the plane of rotation and the axial chip area is related to the axial force component acting along the axis of cutter rotation. In contrast to the typical approach, the rake face chip area (see the gray region in Fig. 1) is not used in the model.

Fig. 2 defines entry and exit angles. Let the angular orientation of any point on the cutting edge be designated θ. The leading point of the tooth enters the cut at the entry angle, θ_{st}, and exits the cut at the exit angle, θ_{ex}. For a given radial immersion, values of θ_{st} and θ_{ex} are obtained using geometrical calculations. These two angles are fixed positions in space with respect to the cutter.

The angular position of the leading point of the p th tooth, taken from an arbitrary reference, is designated θ_p, and is illustrated in Fig. 2. This is the independent variable for the force model proposed in this paper. In steady state, stable machining, the cutting forces are cyclic over a period of one complete revolution of the cutter. The term "instantaneous" will be taken to refer to the current angular position of the p th tooth, θ_p.

The angular position, θ, of any general point inside the tool-chip contact zone, is a function of θ_p. Let the angular positions of the leading and trailing points of the tool chip contact zone be designated θ_L and θ_T respectively. To visualize the relationships

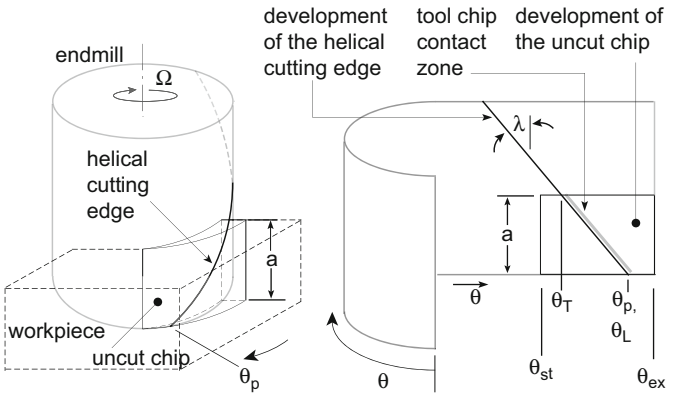

Fig. 2. Development of a representative helical cutting edge and the corresponding uncut chip. θ is the angular orientation of any point on the tool chip contact zone, or on the cutting edge (from an arbitrary reference). θ_L and θ_T are leading and trailing points of the tool chip contact zone, respectively. The tool tip is at θ_p. The entry and exit angles (θ_{st} and θ_{ex}) are fixed angular orientations.

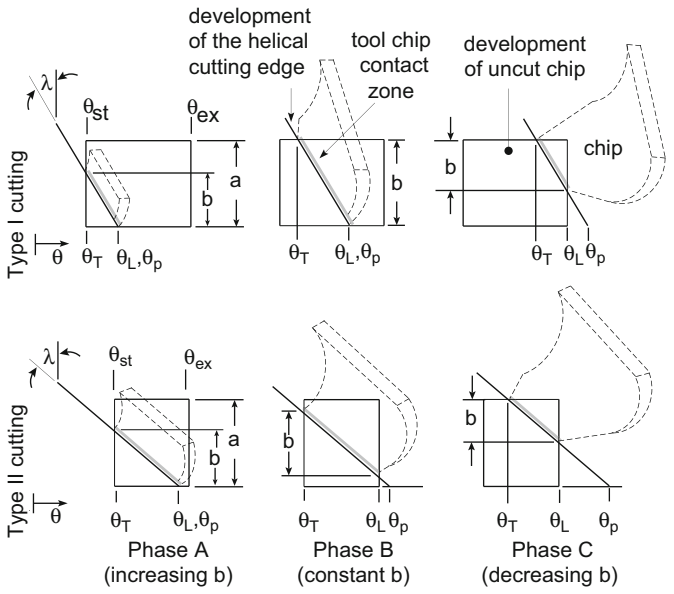

Fig. 3. Progress of tool chip contact zone as the helical endmill rotates. In Type I cutting, $b=a$, during Phase B of the cut. In Type II cutting, $b<a$, always.

between the variables, it is convenient to study the development of the cylindrical surface of the endmill and the uncut chip as shown in Fig. 2. As the cutter rotates, the tool chip contact zone evolves as shown in Fig. 3. Two different types of cutting may occur, designated Type I and Type II, after Tlusty and MacNeil [22], which are established based on the following conditions:

$$\text{Type I cutting}: \quad a\tan\lambda \le (D/2)(\theta_{ex}-\theta_{st}) \tag{2}$$

$$\text{Type II cutting}: \quad a\tan\lambda > (D/2)(\theta_{ex}-\theta_{st}) \tag{3}$$

Each type of cutting is divided into three phases, called A,B and C, after Tlusty and MacNeil [22], as shown in Fig. 3. The solution presented here treats all these phases as a single one. A single expression for b covers all the phases. Algebra takes care of the conditions governed by Eqs. (2) and (3).

In Section 2.1 the basis is established to express the chip width and chip thickness as functions of θ_p with the help of intermediate variables θ_L and θ_T. Analytic expressions are derived for θ_L, θ_T, b, and h, as functions of θ_p. Based on those expressions, the chip areas are found as functions of θ_p when building the force model.

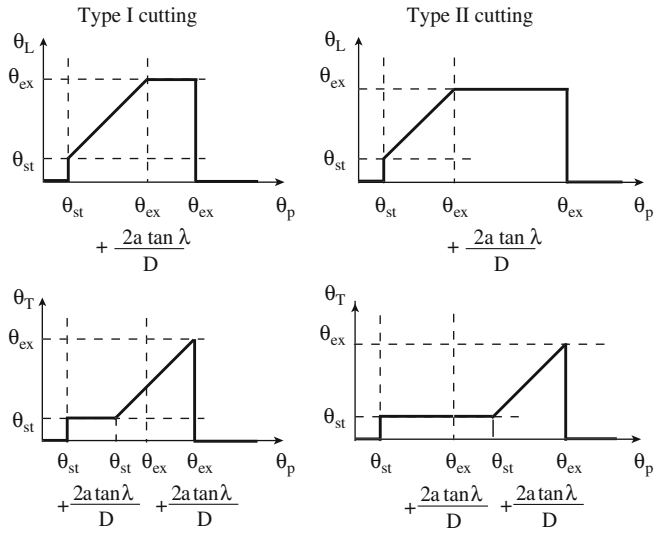

Fig. 4. Evolution of the intermediate variables θ_L and θ_T as functions of θ_p in Type I and Type II cutting. The functional relationships are obtained by inspection of Fig. 3.

By inspection of Fig. 3, it is possible to deduce the variations of θ_L and θ_T for an individual tooth. The relationships are displayed in Fig. 4 in which θ_L and θ_T are plotted as functions of θ_p. Similar plots can also be made for the chip width, b.

2.1. Analytical expressions for θ_L, θ_T, and chip width, b

Compact expressions for θ_L, θ_T, and b, as functions of θ_p, may be obtained based on two alternative formulations presented here, the Heaviside unit step function formulation and the Fourier trigonometric series formulation.

2.1.1. Heaviside unit step function formulation

Inspection of Fig. 4 reveals that, within the domain $\theta_p \in [0,2\pi)$, the functions θ_L, θ_T, and b are made up of finite line segments. These may be conveniently expressed in terms of unit step functions. In this paper, the following definition of the Heaviside unit step function is adopted:

$$H(\theta_p-\varsigma)=\begin{cases}1, & \theta_p \ge \varsigma,\\ 0, & \theta_p < \varsigma,\end{cases} \quad \theta_p \in [0,2\pi) \tag{4}$$

where ς is some fixed value of θ_P. This defines the function as single valued everywhere in the domain.

The unit step function based expressions for θ_L and θ_T are written by inspection of Fig. 4. The equations for the individual straight line segments for θ_L are shown in the Appendix for illustration. The equations of the straight line segments are multiplied by a suitable difference of the step functions. The resulting functional relationships are as follows:

$$\theta_L = \left[\begin{array}{l}\theta_p\{H(\theta_p-\theta_{st})-H(\theta_p-\theta_{ex})\}\\ \quad +\theta_{ex}\left\{H(\theta_p-\theta_{ex})-H\left(\theta_p-\theta_{ex}-\dfrac{2a\tan\lambda}{D}\right)\right\}\end{array}\right] \tag{5}$$

$$\theta_T = \left[\begin{array}{l}\theta_{st}\left\{H(\theta_p-\theta_{st})-H\left(\theta_p-\theta_{st}-\dfrac{2a\tan\lambda}{D}\right)\right\}\\ \quad +\left(\theta_p-\dfrac{2a\tan\lambda}{D}\right)\left\{\begin{array}{l}H\left(\theta_p-\theta_{st}-\dfrac{2a\tan\lambda}{D}\right)\\ \quad -H\left(\theta_p-\theta_{ex}-\dfrac{2a\tan\lambda}{D}\right)\end{array}\right\}\end{array}\right] \tag{6}$$

For a constant helix endmill, with helix angle λ and diameter D, machining with a fixed value of the commanded axial depth of cut, a, the chip width, b, may be obtained by inspection of Fig. 3

$$b = [(D/2)\cot\lambda](\theta_L - \theta_T) \tag{7}$$

2.1.2. Fourier trigonometric series formulation

Since the patterns for θ_L, θ_T, and b repeat once every revolution, yielding a fundamental angular period of 2π, it is possible to write these functions in trigonometric series with appropriate Fourier coefficients.

Trigonometric series expansions for angular position of the leading and trailing points of the tool-chip contact may be written as follows:

$$\theta_L = L_0 + \sum_{k=1}^{\infty} \{L_k \cos(k\theta_p) + M_k \sin(k\theta_p)\} \tag{8}$$

$$\theta_T = T_0 + \sum_{k=1}^{\infty} \{T_k \cos(k\theta_p) + R_k \sin(k\theta_p)\} \tag{9}$$

where L_0, L_k, M_k and T_0, T_k, R_k are the relevant Fourier coefficients.

Eq. (7) from the Heaviside formulation still holds. Therefore, for the purpose of computation, a separate expression for b need not be derived. However, in some applications, especially if the intent is to study the variation of b alone,[2] it is more economical to compute just a single set of Fourier coefficients, instead of two sets for θ_L and θ_T. Thus, b may be expressed in a trigonometric series:

$$b = B_0 + \sum_{k=1}^{\infty} \{B_k \cos(k\theta_p) + C_k \sin(k\theta_p)\} \tag{10}$$

where B_0, B_k, C_k are the relevant Fourier coefficients.

The Fourier coefficients may be derived using standard techniques by piecewise integrations over the period $\theta_p \in [0,2\pi)$ based on the variations displayed in Fig. 4. The details are relegated to the Appendix.

Average Fourier coefficients in Eqs. (8)–(10) are

$$L_0 = \frac{1}{2\pi}\left[\frac{(\theta_{ex}^2 - \theta_{st}^2)}{2} + \frac{2a\tan\lambda}{D}\theta_{ex}\right] \tag{11}$$

$$T_0 = \frac{1}{2\pi}\left[\frac{(\theta_{ex}^2 - \theta_{st}^2)}{2} + \frac{2a\tan\lambda}{D}\theta_{st}\right] \tag{12}$$

$$B_0 = \frac{a(\theta_{ex} - \theta_{st})}{2\pi} \tag{13}$$

Results of the calculations for L_k, M_k, T_k, R_k, B_k and C_k are listed in Table 1. For instance, the coefficient, L_k, may be formed by inspection of column 2 of Table 1 which shows that L_k has four terms in the summation:

$$L_k = \frac{1}{\pi}\left[\begin{array}{l} -\dfrac{\theta_{st}}{k}\sin(k\theta_{st}) - \dfrac{1}{k^2}\cos(k\theta_{st}) \\ \quad + \dfrac{1}{k^2}\cos(k\theta_{ex}) + \dfrac{\theta_{ex}}{k}\sin\left[k\left(\theta_{ex} + \dfrac{2a\tan\lambda}{D}\right)\right] \end{array}\right] \tag{14}$$

The same approach is used for M_k, T_k, R_k, B_k and C_k. The trigonometric series formulation includes an infinite sum. In practice, a partial Fourier summation may be applied, which necessitates the truncation of the series.

[2] Yang et al. [25] have offered an interesting study of depth-of-cut variations in end milling. Xu et al. [24] have presented a study of depth-of-cut variations in ball end milling.

Table 1
Construction of Fourier coefficients L_k, M_k, T_k, R_k, B_k and C_k.

Terms comprising the Fourier sum	Coefficients of the terms in col.1 of this table					
	L_k	M_k	T_k	R_k	B_k	C_k
$\sin[k(\theta_{st})]$	$-\frac{\theta_{st}}{\pi k}$	$-\frac{1}{\pi k^2}$	$-\frac{\theta_{st}}{\pi k}$	0	0	$-\frac{D\cot\lambda}{2\pi k^2}$
$\cos[k(\theta_{st})]$	$-\frac{1}{\pi k^2}$	$\frac{\theta_{st}}{\pi k}$	0	$\frac{\theta_{st}}{\pi k}$	$-\frac{D\cot\lambda}{2\pi k^2}$	0
$\sin[k(\theta_{ex})]$	0	$\frac{1}{\pi k^2}$	0	0	0	$\frac{D\cot\lambda}{2\pi k^2}$
$\cos[k(\theta_{ex})]$	$\frac{1}{\pi k^2}$	0	0	0	$\frac{D\cot\lambda}{2\pi k^2}$	0
$\sin\left[k\left(\theta_{st}+\frac{2a\tan\lambda}{D}\right)\right]$	0	0	0	$-\frac{1}{\pi k^2}$	0	$\frac{D\cot\lambda}{2\pi k^2}$
$\cos\left[k\left(\theta_{st}+\frac{2a\tan\lambda}{D}\right)\right]$	0	$-\frac{\theta_{ex}}{\pi k}$	$-\frac{1}{\pi k^2}$	0	$\frac{D\cot\lambda}{2\pi k^2}$	0
$\sin\left[k\left(\theta_{ex}+\frac{2a\tan\lambda}{D}\right)\right]$	$\frac{\theta_{ex}}{\pi k}$	0	$\frac{\theta_{ex}}{\pi k}$	$\frac{1}{\pi k^2}$	0	$-\frac{D\cot\lambda}{2\pi k^2}$
$\cos\left[k\left(\theta_{ex}+\frac{2a\tan\lambda}{D}\right)\right]$	0	0	$\frac{1}{\pi k^2}$	$-\frac{\theta_{ex}}{\pi k}$	$-\frac{D\cot\lambda}{2\pi k^2}$	0

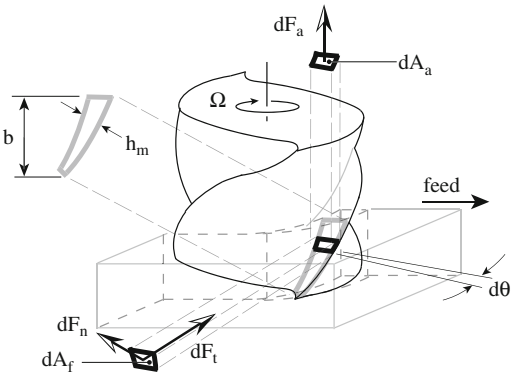

Fig. 5. The differential frontal projected chip area, dA_f, is related to the differential force components in the plane, dF_t (tangential), and dF_n (normal). The differential projected axial chip area, dA_a, is related to the differential axial force component, dF_a. The rake face chip area (the gray region, labeled with b and h_m) is not used in the model. A two fluted, right handed endmill is illustrated.

2.2. Analytical expressions for chip thickness

Fig. 5 displays an instantaneous shape of the chip cross section. The radial chip thickness is designated as h, and it can be seen that this parameter varies for different angular orientations of the tool. The true path of the milling tooth, in the plane, is trochoidal. Martellotti's [14] simplified circular tool path approximation is used here because it is common practice and yields good results. For any angular orientation, θ, the chip thickness based on the circular path approximation is

$$h(\theta) = f_T \sin\theta \tag{15}$$

where f_T is the feed per tooth.

For a helical cutter, the (instantaneous) mean chip thickness, h_m (shown in Fig. 5) is a function of θ_p, and may be calculated as follows:

$$h_m = \frac{1}{\theta_T - \theta_L}\int_{\theta_L}^{\theta_T} f_T \sin\theta \, d\theta \tag{16}$$

Upon simplification,

$$h_m = f_T \sin\left[\frac{\theta_L + \theta_T}{2}\right]\mathrm{sinc}\left[\frac{\theta_T - \theta_L}{2}\right] \triangleq f_T \xi_h \tag{17}$$

where the symbol ξ_h is shorthand notation and the sampling function (sine cardinal) is defined as

$$\mathrm{sinc}(\varsigma) \triangleq \frac{\sin(\varsigma)}{\varsigma} \tag{18}$$

For the complete tooth passage across the chip, the averaged mean chip thickness, $\overline{h}_m$, is found by averaging h_m over the span of angular tool-chip contact (θ_{span}):

$$\overline{h}_m = \frac{1}{\theta_{span}} \int_{\theta_{st}}^{\theta_{ex}+2a\tan\lambda/D} h_m(\theta_p)\, d\theta_p = \frac{f_T}{\theta_{span}} \int_{\theta_{st}}^{\theta_{ex}+2a\tan\lambda/D} \xi_h\, d\theta_p \tag{19}$$

where

$$\theta_{span} \triangleq \theta_{ex} + \frac{2a\tan\lambda}{D} - \theta_{st} \tag{20}$$

In this section, the shape of the chip, characterized by the chip width and chip thickness, has been analytically expressed as a function of the angular position of the p th tooth, θ_p. These expressions are used in characterizing the chip area in the force model to be developed in the forthcoming section, and also used in the cutting coefficient formulation which will follow.

3. Force model for helical peripheral milling

In this section a new model for cutting forces in helical peripheral milling is developed. Since this is a mechanistic model, the chip area must be related to the cutting forces. It is a rigid model because the effects of tool or part deflections on the chip area are ignored.

Fig. 5 shows the scheme which is chosen to relate the three differential cutting force components to the respective areas. The differential projected frontal chip area, dA_f, is related to the differential tangential force component, dF_t, and the differential normal force component, dF_n. The differential projected axial chip area, dA_a, is related to the differential axial force component, dF_a. In contrast to the typical approach (e.g., [7]) the rake face chip area (the gray region in Fig. 5) is not used in the model.

3.1. Force model for a single toothed cutter

Empirical relationships yield the tangential, normal, and axial components of the differential elements of force for the mechanistic model

$$\begin{Bmatrix} dF_t \\ dF_n \\ dF_a \end{Bmatrix} = \begin{pmatrix} dA_f & 0 & 0 \\ 0 & dA_f & 0 \\ 0 & 0 & dA_a \end{pmatrix} \begin{Bmatrix} K_{tc} \\ K_{nc} \\ K_{ac} \end{Bmatrix} \tag{21}$$

where K_{tc}, K_{nc} and K_{ac} are linearized cutting coefficients which may be obtained experimentally during the process model calibration for any specific situation.

For practical purposes, such as measurement of the cutting force components, it is convenient to calculate force components in a fixed frame of reference. A rectangular Cartesian coordinate system is chosen here with the positive x-axis oriented in the direction of the feed. The z-axis is aligned with the axis of the cutter. Thus, F_x is the feed force, F_y the transverse force, and F_z is the axial thrust force. A left handed system is chosen. This choice is arbitrary, following Tlusty [21, Chapter 9, Section 9.5.4, p. 549], and has no physical significance.

The rotating (tangential and normal) components are related to components in a fixed coordinate frame in the plane (x–y) via a rotation matrix, while the axial component remains decoupled:

$$\begin{Bmatrix} dF_x \\ dF_y \\ dF_z \end{Bmatrix} = \begin{Bmatrix} dF_{tx}+dF_{nx} \\ dF_{ty}+dF_{ny} \\ dF_a \end{Bmatrix} = \begin{pmatrix} \cos\theta & \sin\theta & 0 \\ \sin\theta & -\cos\theta & 0 \\ 0 & 0 & 1 \end{pmatrix} \begin{Bmatrix} dF_t \\ dF_n \\ dF_a \end{Bmatrix} \tag{22}$$

Substituting from Eq. (21) and integrating yields the total forces:

$$\begin{Bmatrix} F_x \\ F_y \\ F_z \end{Bmatrix} = \begin{pmatrix} \int \cos\theta dA_f & \int \sin\theta dA_f & 0 \\ \int \sin\theta dA_f & -\int \cos\theta dA_f & 0 \\ 0 & 0 & \int dA_a \end{pmatrix} \begin{Bmatrix} K_{tc} \\ K_{nc} \\ K_{ac} \end{Bmatrix} \tag{23}$$

where the integrations are carried out over the appropriate limits. These limits are explicitly shown in a subsequent step, after applying certain transformations.

To compute the integrals $\int \sin\theta\, dA_f$ and $\int \cos\theta\, dA_f$ in Eq. (23), a local coordinate, ζ, has been invoked in Fig. 6(a). By inspection of the geometry:

$$d\zeta = \left(\frac{b}{\theta_T - \theta_L}\right) d\theta \tag{24}$$

Again, from Fig. 6(a), the differential element of frontal chip area, dA_f, is

$$dA_f = h\, d\zeta = f_T \sin\theta\, d\zeta \tag{25}$$

where the local chip thickness at θ is obtained using the circular path approximation, $h = f_T \sin\theta$ [Eq. (15)].

Eliminating $d\zeta$ using Eq. (24) yields dA_f as a function of θ:

$$dA_f = \left(\frac{b f_T}{\theta_T - \theta_L}\right) \sin\theta\, d\theta \tag{26}$$

Based on Fig. 6(b), the differential element of the projected axial chip area, dA_a, is

$$dA_a = h\frac{D}{2} d\theta = \frac{D f_T}{2} \sin\theta\, d\theta \tag{27}$$

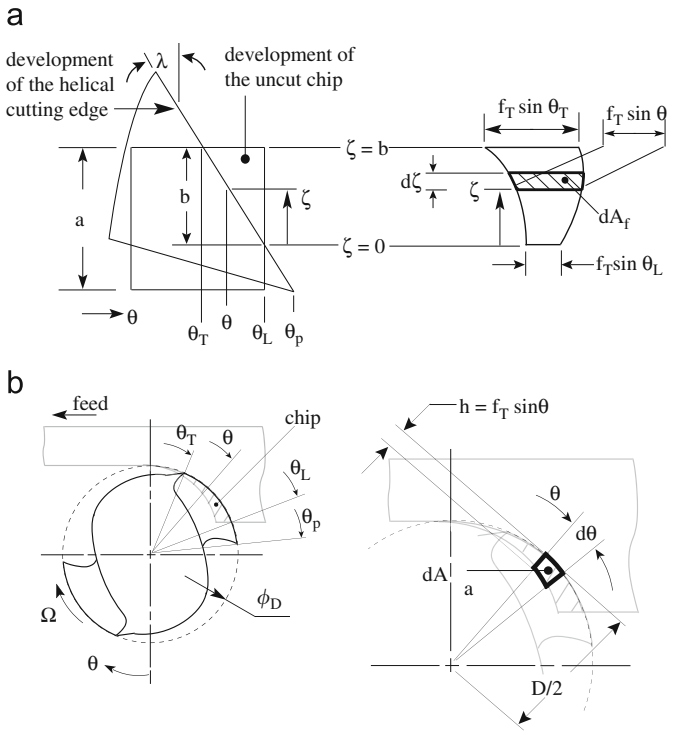

Fig. 6. Differential elements of (a) the projected frontal chip area, dA_f, and (b) the projected axial chip area, dA_a.

The three integrals $\int \sin\theta\, dA_f$, $\int \cos\theta\, dA_f$ and $\int dA_a$ may now be computed:

$$\int \sin\theta\, dA_f = \left(\frac{bf_T}{\theta_T-\theta_L}\right)\int_{\theta_L}^{\theta_T} \sin^2\theta\, d\theta \tag{28}$$

$$\int \cos\theta\, dA_f = \left(\frac{bf_T}{\theta_T-\theta_L}\right)\int_{\theta_L}^{\theta_T} \sin\theta\cos\theta\, d\theta \tag{29}$$

$$\int dA_a = \frac{Df_T}{2}\int_{\theta_L}^{\theta_T} \sin\theta\, d\theta \tag{30}$$

These three results may be substituted into Eq. (23) to obtain, upon simplification:

$$\begin{Bmatrix} F_x \\ F_y \\ F_z \end{Bmatrix} = f_T \begin{pmatrix} b\xi_1 & b\xi_2 & 0 \\ b\xi_2 & -b\xi_1 & 0 \\ 0 & 0 & D\xi_3 \end{pmatrix} \begin{Bmatrix} K_{tc} \\ K_{nc} \\ K_{ac} \end{Bmatrix} \tag{31}$$

where

$$\xi_1 = \sin\left[\frac{\theta_T+\theta_L}{2}\right]\cos\left[\frac{\theta_T+\theta_L}{2}\right]\cos\left[\frac{\theta_T-\theta_L}{2}\right]\mathrm{sinc}\left[\frac{\theta_T-\theta_L}{2}\right] \tag{32}$$

$$\xi_2 = \tfrac{1}{2}[1-\cos(\theta_T+\theta_L)\ \mathrm{sinc}\ (\theta_T-\theta_L)] \tag{33}$$

and

$$\xi_3 = \sin\left[\frac{\theta_T+\theta_L}{2}\right]\sin\left[\frac{\theta_T-\theta_L}{2}\right] \tag{34}$$

where the sampling function (sinc) has been defined earlier in Eq. (18).

In the above equations, the variables θ_L, θ_T and b are functions of θ_p. The functional expressions for θ_L, θ_T and b have been derived in the earlier section. Eq. (31) represents the force components on a single tooth, as a function of θ_p, in closed form.

3.2. Modeling for multiple teeth

In a multiple toothed cutter, the components of the total force are a summation of the force components of the individual teeth

$$\begin{Bmatrix} F_X \\ F_Y \\ F_Z \end{Bmatrix} = \begin{Bmatrix} \sum_{i=1}^{N} F_x(\overline{\theta_p-\chi_i}, f_{T_i}) \\ \sum_{i=1}^{N} F_y(\overline{\theta_p-\chi_i}, f_{T_i}) \\ \sum_{i=1}^{N} F_z(\overline{\theta_p-\chi_i}, f_{T_i}) \end{Bmatrix} \tag{35}$$

where F_X, F_Y and F_Z are the components of the total force, χ_i is the pitch angle of the i th tooth w.r.t. the p th tooth, f_{T_i} is the feed/tooth associated with the i th tooth, N is the number of teeth in the cutter, and p is the arbitrary ($1 \le p \le N$), being just a reference.

For uniformly spaced teeth, χ_i has a constant value. For differential tooth spacing the tooth pitch angles, χ_i, are directly obtained from the specifications of the endmill. The effective feeds per tooth, f_{T_i}, are found by dividing the feed per revolution in proportion with the angular tooth spacings of successive teeth.

Runout affects the feeds, f_{T_i} [9]. For simplicity, consider a two fluted cutter. Let f_{T_1} and f_{T_2} be the effective feeds per tooth experienced by the two teeth, and f_T be the nominal (commanded) feed per tooth. Let the total indicated reading (TIR), upon mounting the endmill in the holder on the spindle, be a measure of the relative runout between the two teeth, designated ρ. The following relations hold (convention $f_{T_1} > f_{T_2}$)

$$f_{T_1} + f_{T_2} = 2f_T \tag{36}$$

$$f_{T_1} - f_{T_2} = |2\rho| \tag{37}$$

Solving Eqs. (36) and (37) simultaneously

$$f_{T_1} = f_T + |\rho| \tag{38}$$

and

$$f_{T_2} = f_T - |\rho| \tag{39}$$

For a cutter with more than two teeth, the expressions for effective feed can be derived using similar arguments.

3.3. Cutting coefficient identification

Cutting coefficients are empirical and are generally determined experimentally. Martellotti [14] proposed that the average undeformed chip thickness could be related to the components of the cutting force. Sawin [17], Salomon [16], and Sabberwal [15] showed that the cutting coefficient varies with the chip thickness.

The coefficients also depend on other process parameters such as cutting speed [19] and tool geometry [8]. For simplicity, the cutting speed, axial depth of cut, and tool geometry are kept fixed in the experiments reported in this paper. Hence, the results reported here hold only for the specific type of tool geometry used, the stated cutting speed, and the axial depth of cut used in the experiments.

Based on [15], the coefficients may be expressed as exponential functions of the averaged mean chip thickness, $\overline{h}_m$, having the general form $K = e^{\Gamma}(\overline{h}_m)^{\Psi}$. Thus, the following set of relations may be written:

$$\begin{Bmatrix} \ln K_{tc} \\ \ln K_{nc} \\ \ln K_{ac} \end{Bmatrix} = \begin{pmatrix} 1 & \ln\overline{h}_m & 0 & 0 & 0 & 0 \\ 0 & 0 & 1 & \ln\overline{h}_m & 0 & 0 \\ 0 & 0 & 0 & 0 & 1 & \ln\overline{h}_m \end{pmatrix} \begin{Bmatrix} \Gamma_{tc} \\ \Psi_{tc} \\ \Gamma_{nc} \\ \Psi_{nc} \\ \Gamma_{ac} \\ \Psi_{ac} \end{Bmatrix} \tag{40}$$

where $\Gamma_{tc,nc,ac}$ and $\Psi_{tc,nc,ac}$ are cutting constants. The values of these constants depend on the combination of tool material and work material, the specific cutting geometry, as well as cutting conditions, such as the type of cutting fluid being used.

The cutting coefficients described above can be experimentally extracted based on a small set of cutting tests. The coefficients $K_{tc,nc,ac}$ corresponding to a given feed per tooth, f_T, may be calculated based on average cutting force components for a chosen set of cutting conditions. For these same conditions, the averaged mean chip thickness, $\overline{h}_m$, may be computed using Eq. (19). The exercise is repeated for a set of different values of f_T. Thus, a mapping is established, generating a functional dependence of $K_{tc,nc,ac}$ on $\overline{h}_m$. These data may be used to obtain appropriate fits to find the cutting constants in Eq. (40).

For a single helical tooth, the components of the cutting force may be averaged over one cutter revolution. The averaged components of the cutting force, $\overline{F}_x$, $\overline{F}_y$, and $\overline{F}_z$, may be expressed as

$$\begin{Bmatrix} \overline{F}_x \\ \overline{F}_y \\ \overline{F}_z \end{Bmatrix} = f_T \left[\frac{1}{2\pi}\int_0^{2\pi} \begin{pmatrix} b\xi_1 & b\xi_2 & 0 \\ b\xi_2 & -b\xi_1 & 0 \\ 0 & 0 & D\xi_3 \end{pmatrix} d\theta_p\right] \begin{Bmatrix} K_{tc} \\ K_{nc} \\ K_{ac} \end{Bmatrix} \tag{41}$$

Using shorthand notation:

$$\begin{Bmatrix} \overline{F}_x \\ \overline{F}_y \\ \overline{F}_z \end{Bmatrix} = \frac{f_T}{2\pi} \begin{pmatrix} I_1 & I_2 & 0 \\ I_2 & -I_1 & 0 \\ 0 & 0 & DI_3 \end{pmatrix} \begin{Bmatrix} K_{tc} \\ K_{nc} \\ K_{ac} \end{Bmatrix} \tag{42}$$

where

$$I_1 \triangleq \int_0^{2\pi} b\xi_1\, d\theta_p, \quad I_2 \triangleq \int_0^{2\pi} b\xi_2\, d\theta_p, \quad I_3 \triangleq \int_0^{2\pi} \xi_3\, d\theta_p \tag{43}$$

Solving for the coefficients yields

$$\begin{Bmatrix} K_{tc} \\ K_{nc} \\ K_{ac} \end{Bmatrix} = \frac{2\pi}{f_T} \begin{pmatrix} \frac{I_1}{I_1^2+I_2^2} & \frac{I_2}{I_1^2+I_2^2} & 0 \\ \frac{I_2}{I_1^2+I_2^2} & \frac{-I_1}{I_1^2+I_2^2} & 0 \\ 0 & 0 & \frac{1}{DI_3} \end{pmatrix} \begin{Bmatrix} \overline{F}_x \\ \overline{F}_y \\ \overline{F}_z \end{Bmatrix} \tag{44}$$

where $\overline{F}_{x,y,z}$ are to be obtained based on experiments, and the integrals need to be evaluated for the corresponding experimental conditions. The integrands in Eq. (43) have closed form expressions {using Eqs. (32)–(34) and Eqs. (5)−(7) or (8)−(10)}.

The cutting coefficients identified above are averaged coefficients, having been derived based on the averaged forces, $\overline{F}_{x,y,z}$, and expressed as functions of the averaged mean chip thickness, $\overline{h}_m$. A set of experiments may be conducted for any fixed value of radial immersion at different feed rates, yielding values of $K_{tc,nc,ac}$ for a range of $\overline{h}_m$. Values of cutting constants can then be obtained using Eq. (40).

It has been noted earlier that the cutting coefficients are not true constants but depend on process parameters. Only the cutting constants are truly invariant. As the tooth progresses through the cut, the instantaneous value of the mean chip thickness, h_m, evolves. So, it is expected that the cutting coefficients also change because they are dependent on the instantaneous h_m [10]. The functional relation governing this dependence has to be deduced.

Since the cutting constants are invariants, it is plausible that the relationship between the instantaneous cutting coefficients and the instantaneous h_m has the form $K = e^{\Gamma} h_m^{\Psi}$, for fixed values of cutting speed, axial depth of cut, and other fixed cutting conditions such as the type of cutting fluid being used. The values of the cutting constants, $\Gamma_{tc,nc,ac}$ and $\Psi_{tc,nc,ac}$, may be found using the average forces as outlined above. The underlying assumption is that the values of the cutting constants identified in this manner can be used to calculate the instantaneous cutting coefficients. The validity of this assumption will be tested by comparison of experimental force signals with predicted forces based on the instantaneous cutting coefficients.

The instantaneous cutting coefficients are functions of θ_p, and may be expressed through the intermediate variables θ_L and θ_T using Eq. (17):

$$K_{tc} = e^{\Gamma_{tc}}(h_m)^{\Psi_{tc}} = e^{\Gamma_{tc}}(f_T\xi_h)^{\Psi_{tc}} = e^{\Gamma_{tc}}\left[f_T \sin\left(\frac{\theta_L+\theta_T}{2}\right)\mathrm{sinc}\left(\frac{\theta_T-\theta_L}{2}\right)\right]^{\Psi_{tc}} \tag{45}$$

$$K_{nc} = e^{\Gamma_{nc}}(h_m)^{\Psi_{nc}} = e^{\Gamma_{nc}}(f_T\xi_h)^{\Psi_{nc}} = e^{\Gamma_{nc}}\left[f_T \sin\left(\frac{\theta_L+\theta_T}{2}\right)\mathrm{sinc}\left(\frac{\theta_T-\theta_L}{2}\right)\right]^{\Psi_{nc}} \tag{46}$$

$$K_{ac} = e^{\Gamma_{ac}}(h_m)^{\Psi_{ac}} = e^{\Gamma_{ac}}(f_T\xi_h)^{\Psi_{ac}} = e^{\Gamma_{ac}}\left[f_T \sin\left(\frac{\theta_L+\theta_T}{2}\right)\mathrm{sinc}\left(\frac{\theta_T-\theta_L}{2}\right)\right]^{\Psi_{ac}} \tag{47}$$

where the sampling function (sinc) is defined in Eq. (18). The reader should note that the same symbols, $K_{tc,nc,ac}$, are used to denote the average as well as instantaneous cutting coefficients. In extracting the cutting constants, the average coefficients are used. Once the cutting constants are available, instantaneous coefficients are used to make force predictions. The context makes it clear which coefficient is to be applied.

In this subsection, a procedure has been developed for the identification of cutting coefficients. The formulation is indifferent to whether the cutting coefficients are a function of helix angle. The expressions are readily computed for any value of radial immersion. Hence, low immersion tests can be used to determine the cutting coefficients. For any given combination of workpiece material, tool material, tool geometry, and cutting conditions such as use of cutting fluid, the cutting coefficients may be experimentally derived. The coefficients are variable as they are a function of chip thickness. So, cutting constants have been invoked which are true invariants.

Cutting coefficients, $K_{tc,nc,ac}$ (alternatively, the cutting constants, $\Gamma_{tc,nc,ac}, \Psi_{tc,nc,ac}$), and the effective feed, f_T, for an individual tooth, are the input parameters for the force model [Eq. (31)] which are subject to variation, due to the fact that they have to be experimentally measured or otherwise estimated. These variances may be quantified and propagated through the force model to place confidence intervals on predicted forces.

4. Uncertainty analysis for predicted forces

Uncertainties in input parameters are evaluated using either a Type A or a Type B analysis [20]. Type A analysis involves a statistical evaluation of the data. Type B analysis is evaluation by any other means. The sources of uncertainty in cutting coefficients or cutting constants arise out of uncertainties in the measurement of average forces or uncertainties in estimation of instantaneous forces. The random effects can be captured in the form of variances and covariances of cutting constants using a Type A analysis. The systematic effects can be captured in the form of variances in cutting coefficients using a Type B analysis (denoted as Type B1 in this paper). The uncertainties in effective feed arise out of uncertainties in the measurement of runout. Single measurements exclude random effects. The systematic effects can be captured using a Type B analysis (denoted Type B2 in this paper).

In this paper the combined uncertainty of force components owing to the random effects on cutting constants is designated u_{cA}. The combined uncertainty of force components owing to the systematic effects of the force measuring instrumentation is designated u_{cB_1}, and that due to the runout measuring instrument is designated u_{cB_2}.

According to [20, pp. 7–8], when a measurand Y is not measured directly, but is computed from N other quantities $X_1, X_2, \ldots, X_N$ using a functional relation:

$$Y = g(X_1, X_2, \ldots, X_N) \tag{48}$$

then an estimate of the measurand, or output quantity Y, denoted by the lowercase y, is found using input estimates $x_1, x_2, \ldots, x_N$ for the N input quantities $X_1, X_2, \ldots, X_N$ using the functional relationship:

$$y = g(x_1, x_2, \ldots, x_N) \tag{49}$$

The combined standard uncertainty of the measurement result y, denoted by $u_c(y)$ is taken to represent the estimated standard deviation of y, and is the positive square root of the estimated variance $u_c^2(y)$ given by

$$u_c^2(y) = \sum_{i=1}^{N} \left(\frac{\partial g}{\partial x_i}\right)^2 u^2(x_i) + 2\sum_{i=1}^{N-1}\sum_{j=i+1}^{N} \frac{\partial g}{\partial x_i}\frac{\partial g}{\partial x_j} u(x_i, x_j) \tag{50}$$

Combined standard uncertainties of predicted cutting forces may be derived using the above equation in which the functional relation "g" is given by Eq. (31), which defines the function governing the force components. The partial derivatives of g, with

respect to the variables which have uncertainties attached to them, are the respective sensitivity coefficients.

4.1. Propagation of Type A uncertainties

The sensitivities with respect to the cutting constants are found by using Eq. (31) together with Eq. (40):

$$\begin{Bmatrix} s_{11} \\ s_{12} \\ s_{13} \\ s_{14} \\ s_{21} \\ s_{22} \\ s_{23} \\ s_{24} \\ s_{35} \\ s_{36} \end{Bmatrix} = \begin{Bmatrix} \partial F_x/\partial \Gamma_c \\ \partial F_x/\partial \Psi_{tc} \\ \partial F_x/\partial \Gamma_{nc} \\ \partial F_x/\partial \Psi_{nc} \\ \partial F_y/\partial \Gamma_{tc} \\ \partial F_y/\partial \Psi_{tc} \\ \partial F_y/\partial \Gamma_{nc} \\ \partial F_y/\partial \Psi_{nc} \\ \partial F_z/\partial \Gamma_{ac} \\ \partial F_z/\partial \Psi_{ac} \end{Bmatrix} = f_T \begin{Bmatrix} b\xi_1 K_{tc} \\ b\xi_1 K_{tc} \ln \bar{h}_m \\ b\xi_2 K_{nc} \\ b\xi_2 K_{nc} \ln \bar{h}_m \\ b\xi_2 K_{tc} \\ b\xi_2 K_{tc} \ln \bar{h}_m \\ -b\xi_1 K_{nc} \\ -b\xi_1 K_{nc} \ln \bar{h}_m \\ D\xi_3 K_{ac} \\ D\xi_3 K_{ac} \ln \bar{h}_m \end{Bmatrix} \tag{51}$$

where the cutting coefficients are parameterized in the cutting constants according to Eq. (40).

These sensitivities are expressed in terms of the cutting coefficients in the above equation because the expressions remain compact when written in this manner. They are functions of the angular position of the pth tooth, θ_p.

The variances of cutting constants due to random effects, available from the Type A evaluation, may be propagated to the predicted forces using Eq. (31) and the sensitivities expressed in Eq. (51) to yield the combined uncertainties $u_{c_A}(f_{x,y,z})$ of predicted forces for a single tooth by applying Eq. (50):

$$\begin{Bmatrix} u^2_{c_A}(f_x) \\ u^2_{c_A}(f_y) \\ u^2_{c_A}(f_z) \end{Bmatrix} = \begin{pmatrix} s^2_{11} & s^2_{12} & s^2_{13} & s^2_{14} & 0 & 0 \\ s^2_{21} & s^2_{22} & s^2_{23} & s^2_{24} & 0 & 0 \\ 0 & 0 & 0 & 0 & s^2_{35} & s^2_{36} \end{pmatrix} \underbrace{\begin{Bmatrix} u^2(\gamma_{tc}) \\ u^2(\psi_{tc}) \\ u^2(\gamma_{nc}) \\ u^2(\psi_{nc}) \\ u^2(\gamma_{ac}) \\ u^2(\psi_{ac}) \end{Bmatrix}}_{\text{estimated variances}}$$
$$+2 \begin{pmatrix} s_{11}s_{12} & s_{11}s_{13} & s_{11}s_{14} & s_{12}s_{13} & s_{12}s_{14} & s_{13}s_{14} & 0 \\ s_{21}s_{22} & s_{21}s_{23} & s_{21}s_{24} & s_{22}s_{23} & s_{22}s_{24} & s_{23}s_{24} & 0 \\ 0 & 0 & 0 & 0 & 0 & 0 & s_{35}s_{36} \end{pmatrix}$$
$$\times \underbrace{\begin{Bmatrix} u(\gamma_{tc},\psi_{tc}) \\ u(\gamma_{tc},\gamma_{nc}) \\ u(\gamma_{tc},\psi_{nc}) \\ u(\psi_{tc},\gamma_{nc}) \\ u(\psi_{tc},\psi_{nc}) \\ u(\gamma_{nc},\psi_{tc}) \\ u(\gamma_{ac},\psi_{ac}) \end{Bmatrix}}_{\text{estimated covariances}} \tag{52}$$

where lowercase $\gamma_{tc,nc,ac}$ and $\psi_{tc,nc,ac}$ are input estimates for the values of input quantities $\Gamma_{tc,nc,ac}$ and $\Psi_{tc,nc,ac}$, respectively, and s_{ij} are the sensitivity coefficients evaluated at the estimated parameters $\gamma_{tc,nc,ac}$ and $\psi_{tc,nc,ac}$.

4.2. Propagation of Type B1 uncertainties

The variances of instantaneous cutting coefficients (obtained using a Type B1 evaluation) are functions of θ_p because the instantaneous forces, and the sensitivities of cutting coefficients to the instantaneous forces, are functions of θ_p. The relation between instantaneous cutting coefficients and instantaneous cutting force components may be obtained by inverting the cutting force Eq. (31) to yield

$$\begin{Bmatrix} K_{tc} \\ K_{nc} \\ K_{ac} \end{Bmatrix} = \frac{1}{f_T} \begin{pmatrix} \dfrac{\xi_1}{[b(\xi_1^2+\xi_2^2)]} & \dfrac{\xi_2}{[b(\xi_1^2+\xi_2^2)]} & 0 \\ \dfrac{\xi_2}{[b(\xi_1^2+\xi_2^2)]} & \dfrac{-\xi_1}{[b(\xi_1^2+\xi_2^2)]} & 0 \\ 0 & 0 & \dfrac{1}{(D\xi_3)} \end{pmatrix} \begin{Bmatrix} F_x \\ F_y \\ F_z \end{Bmatrix} \tag{53}$$

Eq. (53) yields the following sensitivity coefficients for use in propagation of the uncertainty in instantaneous force measurements to the uncertainties in instantaneous cutting coefficients:

$$\begin{Bmatrix} s_{tx} \\ s_{ty} \\ s_{nx} \\ s_{ny} \\ s_{az} \end{Bmatrix} = \begin{Bmatrix} \partial K_{tc}/\partial F_x \\ \partial K_{tc}/\partial F_y \\ \partial K_{nc}/\partial F_x \\ \partial K_{nc}/\partial F_y \\ \partial K_{ac}/\partial F_z \end{Bmatrix} = \frac{1}{f_T} \begin{Bmatrix} \xi_1/[b(\xi_1^2+\xi_2^2)] \\ \xi_2/[b(\xi_1^2+\xi_2^2)] \\ \xi_2/[b(\xi_1^2+\xi_2^2)] \\ -\xi_1/[b(\xi_1^2+\xi_2^2)] \\ 1/(D\xi_3) \end{Bmatrix} \tag{54}$$

Using the above sensitivities in Eq. (50), the variances of cutting coefficients, due to the systematic effects, are

$$\begin{Bmatrix} u^2(k_{tc}) \\ u^2(k_{nc}) \\ u^2(k_{ac}) \end{Bmatrix} = \begin{pmatrix} s^2_{tx} & s^2_{ty} & 0 \\ s^2_{nx} & s^2_{ny} & 0 \\ 0 & 0 & s^2_{az} \end{pmatrix} \begin{Bmatrix} u^2(f_x) \\ u^2(f_y) \\ u^2(f_z) \end{Bmatrix} \tag{55}$$

where $u^2(f_{x,y,z})$ are the variances of instantaneous force components. The values of $u(f_{x,y,z})$ in Eq. (55) are set at 1.207% of the nominal values of the instantaneous force components based on estimates provided by the force measuring instrument manufacturer [4] who is certified to ISO 9001 and ISO 17025 (for calibration). According to the manufacturer's certificate, the total uncertainty of force measurement using multicomponent dynamometers having piezoelectric charge devices, is calculated as $\sqrt{u^2(\text{force range})+u^2(\text{charge})}$. For forces of 0…60,000 lbf, the uncertainty is 0.5%, and for charge of 0…50,000 pC, uncertainty is 0.5%, which yields $\sqrt{(0.5)^2+(0.5)^2} \simeq 0.707\%$. For the charge amplifier in the measuring chain, the typical uncertainty in these ranges is $<0.5\%$ and should be added to the 0.707%. Thus, the worst case uncertainty is stated at 0.707+0.5=1.207%. For the sake of simplicity, any possible correlation between K_{tc} and K_{nc} from measurement channel cross talk is neglected, i.e., $u(k_{tc},k_{nc})$ is set to zero. Thus the variances in cutting coefficients have been obtained using a Type B1 evaluation.

The sensitivities of cutting forces, with respect to the cutting coefficients, are found using Eq. (31):

$$\begin{Bmatrix} s_{x_{Kt}} \\ s_{x_{Kn}} \\ s_{y_{Kt}} \\ s_{y_{Kn}} \\ s_{z_{Ka}} \end{Bmatrix} = \begin{Bmatrix} \partial F_x/\partial K_{tc} \\ \partial F_x/\partial K_{nc} \\ \partial F_y/\partial K_{tc} \\ \partial F_y/\partial K_{nc} \\ \partial F_z/\partial K_{ac} \end{Bmatrix} = f_T \begin{Bmatrix} b\xi_1 \\ b\xi_2 \\ b\xi_2 \\ -b\xi_1 \\ D\xi_3 \end{Bmatrix} \tag{56}$$

The variances of cutting coefficients due to measurement uncertainties are available from Eq. (55) based on the Type B1 evaluation. These uncertainties may be propagated to the predicted forces using Eq. (31) and the sensitivities expressed in Eq. (56) to yield the combined uncertainties $u_{c_{B1}}(f_{x,y,z})$ of predicted forces for a single tooth by applying Eq. (50):

$$\begin{Bmatrix} u^2_{c_{B1}}(f_x) \\ u^2_{c_{B1}}(f_y) \\ u^2_{c_{B1}}(f_z) \end{Bmatrix} = \begin{pmatrix} s^2_{xKt} & s^2_{xKn} & 0 \\ s^2_{yKt} & s^2_{yKn} & 0 \\ 0 & 0 & s^2_{zKa} \end{pmatrix} \begin{Bmatrix} u^2(k_{tc}) \\ u^2(k_{nc}) \\ u^2(k_{ac}) \end{Bmatrix} \tag{57}$$

where measurement channel cross talk is neglected, i.e., $u(k_{tc},k_{nc})$ is set to zero.

4.3. Propagation of Type B2 uncertainties

Eqs. (38) and (39) yield the following sensitivity coefficients for use in propagation of the uncertainty in relative runout to the uncertainties in effective feeds for individual teeth for a two fluted endmill:

$$\frac{\partial f_{T_1}}{\partial \rho}=1 \quad \text{and} \quad \frac{\partial f_{T_2}}{\partial \rho}=-1 \tag{58}$$

and similar expressions may be written for an endmill with more teeth.

Let $u^2(\rho)$ be the estimated variance in the measured value of relative radial runout of successive teeth. The sensitivities in Eq. (58) may be used in Eq. (50) to estimate the variances of the effective feeds for each individual tooth:

$$u^2(f_{T_1})=\left(\frac{\partial f_{T_1}}{\partial \rho}\right)^2 u^2(\rho)=u^2(\rho) \tag{59}$$

$$u^2(f_{T_2})=\left(\frac{\partial f_{T_2}}{\partial \rho}\right)^2 u^2(\rho)=u^2(\rho) \tag{60}$$

where $u^2(\rho)$ has to be estimated.

The sensitivities of cutting force components with respect to the effective feeds are found using Eq. (31):

$$\begin{Bmatrix} s_{xf} \\ s_{yf} \\ s_{zf} \end{Bmatrix} = \begin{Bmatrix} \partial F_x/\partial f_T \\ \partial F_y/\partial f_T \\ \partial F_z/\partial f_T \end{Bmatrix} = \begin{pmatrix} b\xi_1 & b\xi_2 & 0 \\ b\xi_2 & -b\xi_1 & 0 \\ 0 & 0 & D\xi_3 \end{pmatrix} \begin{Bmatrix} (1+\Psi_{tc})K_{tc} \\ (1+\Psi_{nc})K_{nc} \\ K_{ac} \end{Bmatrix} \tag{61}$$

The uncertainties in the effective feed rates of the i th tooth, as expressed in Eqs. (59) and (60), may be propagated to the predicted forces using Eq. (31) and the sensitivities expressed in Eq. (61) to yield the combined uncertainties $u_{c_{B2}}(f_{x,y,z})$ of the forces for the i th tooth:

$$\begin{Bmatrix} u^2_{c_{B2}}(f_x) \\ u^2_{c_{B2}}(f_y) \\ u^2_{c_{B2}}(f_z) \end{Bmatrix} = u^2(f_{T_i}) \begin{Bmatrix} [s_{xf}]^2 \\ [s_{yf}]^2 \\ [s_{zf}]^2 \end{Bmatrix} \tag{62}$$

In the preceding discussion, an analytical method of quantifying the variances in the model input parameters has been outlined. During the process of experimental determination of the input parameters, their variances and covariances, are to be estimated. A suitable method of calculating the expanded uncertainty, for a desired confidence interval on the predicted forces, has to be established. These aspects are addressed in the next section.

5. Experimental verification of the force model

To verify the predictive capability of the model, the input parameters, namely the cutting coefficients, and radial runout, were determined experimentally. Experimental measurements are subject to uncertainty. The uncertainties in model input parameters were determined and their propagation through the force model was quantified. The analytical cutting force model was then used to predict cutting forces, for various combinations of radial immersion and feed, with 95% confidence intervals placed on force predictions. The predicted force signals were verified against experimental data to validate the model. A 2-fluted, 45° helix, equispaced tooth endmill was used.

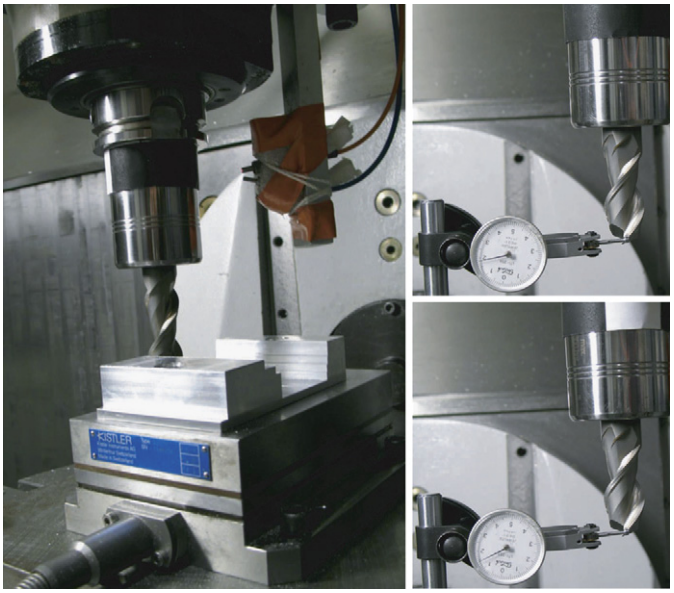

Fig. 7. Experimental set-up showing the helical endmill held in a polygonal chuck, the laser tachometer, and the workpiece mounted on the dynamometer (left). Measurement of runout using a dial indicator is also shown (right).

Table 2
Experimental cutting conditions: dry cutting of aluminum alloy 6061-T6 using a TiB_2 coated solid carbide endmill (Kennametal catalog No. HPF45A750S2150) having two equispaced teeth mounted in a polygonal chuck (Schunk catalog No. 203794).

Endmill diameter (mm)	Helix angle (deg.)	Cutting speed (m/min)	No. of teeth	Axial depth of cut (mm)
19.05	45	250	2	4

Fig. 7 shows the experimental set-up. The machine was a Mikron[3] UCP Vario 5-axis machining center. The specifications of the endmill and toolholder are given in the caption of Table 2. Spindle adaption was hollow shank, taper and face contact HSK-63A. Upon clamping the tool in the spindle, the static radial runout was measured by indicating the endmills with a dial gage having a least count of 2.5 μm (0.0001 in). A three component Kistler dynamometer, model 9257B, was used to measure the three components of the force. Data were acquired using a National Instruments 12-bit data acquisition card at a sampling frequency of 60 kHz. A Tetrahertz Technologies laser tachometer was used to record a synchronizing phasor signal to help estimate the point of entry into the cut for one of the flutes in the endmill.

5.1. Partial radial immersion experiments

Cutting coefficients were extracted for dry machining the aluminum alloy 6061-T6. A 25% radial immersion experiment was used. This was to demonstrate one of the advantages of this analytical model which is that a full immersion experiment is not required to extract cutting coefficients.

The fixed conditions of the experiments are given in Table 2. The averaged mean chip thickness can be varied by changing the feed based on Eq. (19). Values of cutting coefficients were recorded for each level of the averaged mean chip thickness,

[3] All commercial products are identified for the sake of completeness. This does not constitute endorsement of any of these products.

and linear regression was used to establish relationships between them. Using these cutting coefficients, force predictions were made with 95% confidence intervals for down milling, up milling, and mixed mode (over 50% radial immersion), and experimentally verified for different values of feed.

5.2. Experimental extraction of cutting coefficients

Eqs. (31), (41), and (44) indicate that the cutting coefficients in the plane (K_{tc} and K_{nc}) are possibly correlated. The axial coefficient is independent. So, the covariances associated with K_{tc} and K_{nc} need to be considered, i.e., it is a multiresponse, multivariate problem. In extracting the axial coefficient, the variance associated with K_{ac} suffices, i.e., it is a univariate problem.

Experiments were conducted at nine different feed rates, within the range 0.025–0.250 mm/tooth, the time traces of force components were recorded, and average force values, ($\bar{f}_x \bar{f}_y \bar{f}_z$), were computed. The experimental estimates of the average cutting force components are represented using the corresponding lower case letters to distinguish sample measures from population measures. At each feed rate, the experiment was repeated five times. Forces were averaged over one rotation, on a per tooth basis. To reduce the variability, the average was taken for 50 successive rotations. Values of K_{tc}, K_{nc}, and K_{ac}, corresponding to each feed rate, were derived using Eq. (44). Thus, nine sets of five data points each were collected for fitting a linear model according to Eq. (40). Two parameters (slope and intercept) were fitted to 45 points, yielding 43 degrees of freedom for each regression.

5.3. Estimation of cutting constants and variance of radial runout

The cutting constants $\Gamma_{tc,nc}$ and $\Psi_{tc,nc}$ of Eq. (40) may be obtained using multiresponse linear regression, whereas the cutting constants Γ_{ac} and Ψ_{ac} can be obtained using simple linear regression. Kurdi [12] has solved a multiresponse regression problem which has a similar mathematical structure, using the theory presented by Zellner [26]. The method fits a linear regression model and enables the evaluation of the variance–covariance matrix between the responses, and the variance–covariance matrix of the random error in the regression model, which permits the extraction of the variance–covariance matrix of the cutting constants (details in the Appendix). The fitted regression lines are displayed in Fig. 8. Based on the regression, the estimated cutting constants $\Gamma_{tc,nc}$ and $\Psi_{tc,nc}$ are calculated and their mean values are given in Table 3. A linear fit was not found suitable for the axial cutting constants {small values of R^2 in linear regression}. The mean value of K_{ac} was fitted.

The variance covariance matrix of the cutting constants $\Gamma_{tc,nc}$ and $\Psi_{tc,nc}$, obtained using the method of Zellner [26], is given in Table 4. The diagonal elements are the variances, and the off diagonal elements are the respective covariances. The variance of the independent cutting constant Γ_{ac} was found to be 0.00678924.[4]

The uncertainty associated with runout measurement is captured using a Type B evaluation as discussed in [20]. The dial indicator used in runout measurement resolves to 0.0025 mm. The cosine error of the lever type indicator is neglected in this analysis. Based on a rectangular (uniform) distribution of the half

[4] The large number of significant figures are carried so as not to be affected by round off errors [5].

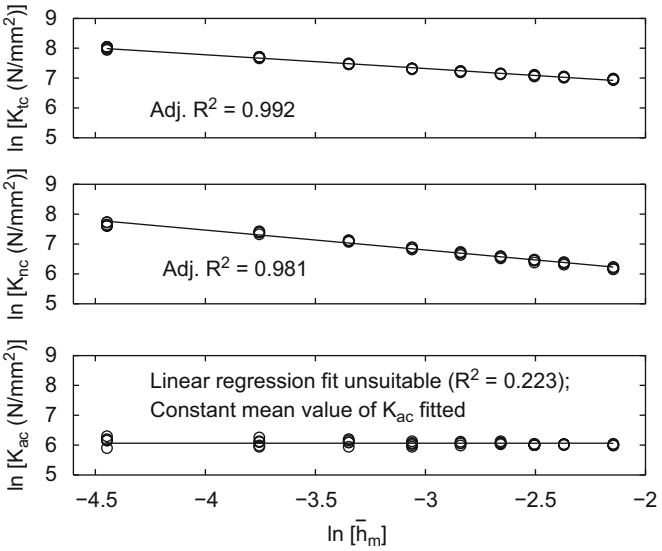

Fig. 8. Linear regression fitting of average cutting coefficients, as a function of the averaged mean chip thickness, for dry milling of 6061-T6 aluminum alloy, using an equispaced tooth, 2-fluted, 45° helix, TiB_2 coated, solid carbide endmill having a nominal radial runout of 10 μm. Experimental points are denoted by " ○ ".

Table 3
Estimated mean cutting constants for cutting conditions of Table 2.

Γ_{tc}	Ψ_{tc}	Γ_{nc}	Ψ_{nc}	Γ_{ac}	Ψ_{ac}
5.928	−0.4634	4.799	−0.6666	6.060	0.000

Table 4
Symmetric variance–covariance matrix of cutting constants for the cutting conditions listed in Table 2.

	Γ_{tc}	Ψ_{tc}	Γ_{nc}	Ψ_{nc}
Γ_{tc}	0.00037172	0.00011714	0.00017171	0.00005411
Ψ_{tc}		0.00003885	0.00005411	0.00001795
Γ_{nc}			0.00184500	0.00058139
Ψ_{nc}				0.00019285

interval, the variance of radial runout measurement is

$$u^2(\rho) = \left(\frac{0.0025}{\sqrt{3}}\right)^2 \tag{63}$$

5.4. Expanded uncertainty

The Type A evaluation of the variances and covariances of the cutting constants was carried out under the assumption of a normal distribution for the measurements and their combined uncertainties. A sufficiently large number of experiments were conducted to yield 43 degrees of freedom for each regression. This indicates that the degrees of freedom for the standard uncertainties of the cutting constants are large enough to justify the choice of the usual coverage factor of 2 for the expanded uncertainty for a 95% confidence interval based on the Student's *t*-distribution [20], i.e., $\kappa_A = 2$.

The Type B evaluation of the standard uncertainties of dynamometer force measurements was carried out based on the manufacturer's certificate under the assumption of a normal distribution for the measurements and their combined uncertainties. It is assumed that the manufacturer's estimate is based on a sufficiently large number of observations to justify the choice of

the usual coverage factor of 2 for the expanded uncertainty for a 95% confidence interval based on the Student's t-distribution, i.e., $\kappa_{B1}=2$.

The Type B evaluation of the standard uncertainties of single measurement estimates of radial runout, using an instrument with a finite resolution, was carried out under the assumption of a uniform distribution for the measurements and their combined uncertainties. The rectangular distribution yields a coverage factor $\kappa_{B2}=1.65$ for a 95% confidence interval.

In the problem at hand, the sources of uncertainty are evaluated by Type A and Type B methods, but their relative magnitudes are not fixed. Turzeniecka [23] has suggested an approximate method to find the expanded uncertainty in such situations. The expanded uncertainty may be computed as the root sum of squares (RSS) of the component expanded uncertainties:

$$U(f)=\sqrt{\kappa_A^2 u_{c_A}^2(f)+\kappa_{B1}^2 u_{c_{B1}}^2(f)+\kappa_{B2}^2 u_{c_{B2}}^2(f)} \tag{64}$$

The predicted forces are

$$\text{Predicted forces}=F_{x,y,z}\pm U(f_{x,y,z})$$

where $F_{x,y,z}$ are calculated based on Eq. (31).

5.5. Force prediction results

Force predictions were made for several combinations of parameters as given in Table 5. The results are displayed in Figs. 9–12. Noteworthy is the fact that magnitudes of the forces, as well as the patterns are predicted accurately. The skewness of the experimental forces in high immersion experiments is also successfully captured. Furthermore, in general, the experimental force patterns were found to lie within the 95% confidence interval bounds even though the dynamics of the force measurement chain, which includes the dynamometer, cable, and amplifier, play a role in introducing high frequency wiggles in force measurements which colors the experimental force signals [3].

5.6. Additional experimental force prediction results

For the sake of compactness, only one set of representative experimental results are reported here. Additional experimental force prediction results are available in [3] where a much larger parameter space (radial immersion, up and down milling configuration) is explored. The reader may be specifically interested in looking at force prediction results using a version of this model based on average cutting coefficients. That model has been validated on two different workpiece materials including the 6061-T6 aluminum alloy as well as a plain carbon steel. Validation also includes the use of two different toolholders (spring collet chuck and elastomeric polygonal chuck), two different tool materials (uncoated carbide and coated carbide), and three different tool geometries (45° helix, 30° helix, and zero helix). In addition, the model has been validated using a differential pitch cutter.

6. Concluding remarks

The fully analytical force model, having a single equation covering the entire domain of angular rotation, is able to predict forces under the practical situations involving radial runout. Only representative results are shown in this paper. For extensive experimental results, including the effects of differential pitch, the reader is referred to [3].

The advantages of the model in cutting coefficient extraction were demonstrated. It was shown that cutting coefficients may be

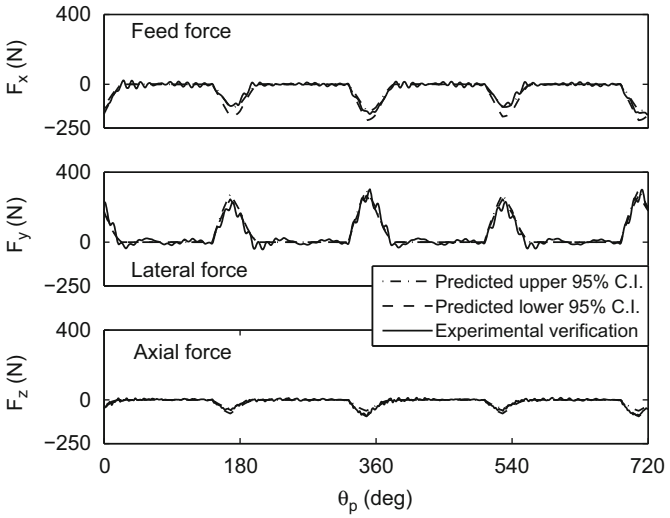

Fig. 9. Predicted vs. experimental force signals: equispaced, 2-fluted, 45° helix cutter; feed 0.100 mm/tooth, 10% radial immersion, down milling. Nominal runout 10 μm. Other conditions as in Table 2.

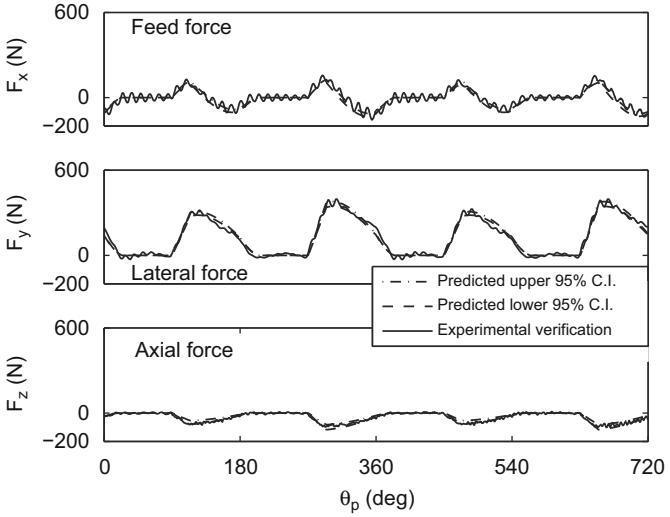

Fig. 10. Predicted vs. experimental force signals: equispaced, 2-fluted, 45° helix cutter; feed 0.050 mm/tooth, 50% radial immersion, down milling. Nominal runout 10 μm. Other conditions as in Table 2.

Table 5
Summary of experimental conditions used to verify force predictions with instantaneous $K_{tc,nc,ac}$, and conditions of Table 2 held fixed.

Results displayed in	Feed (mm/tooth)	Radial immersion (%)	Up/down milling or mixed mode (> 50% *RI*)
Fig. 9	0.100	10	Down milling
Fig. 10	0.050	50	Down milling
Fig. 11	0.050	75	Mixed, cut ends with $h=0$
Fig. 12	0.100	100	Slotting

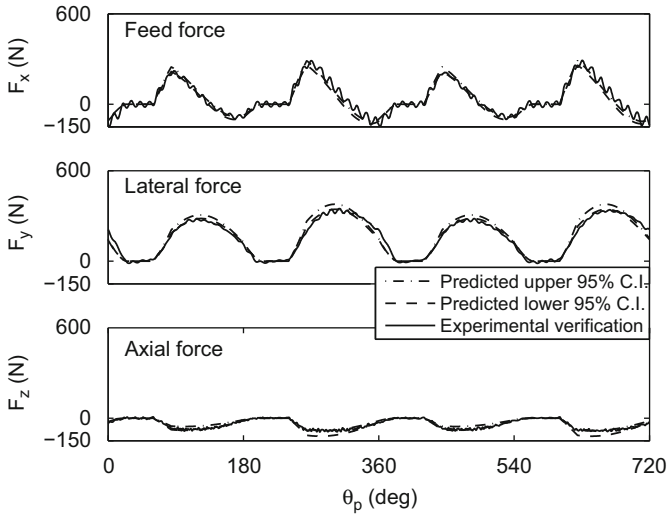

Fig. 11. Predicted vs. experimental force signals: equispaced, 2-fluted, 45° helix cutter; feed 0.050 mm/tooth, 75% radial immersion, cut ends with $h=0$. Nominal runout 10 μm. Other conditions as in Table 2.

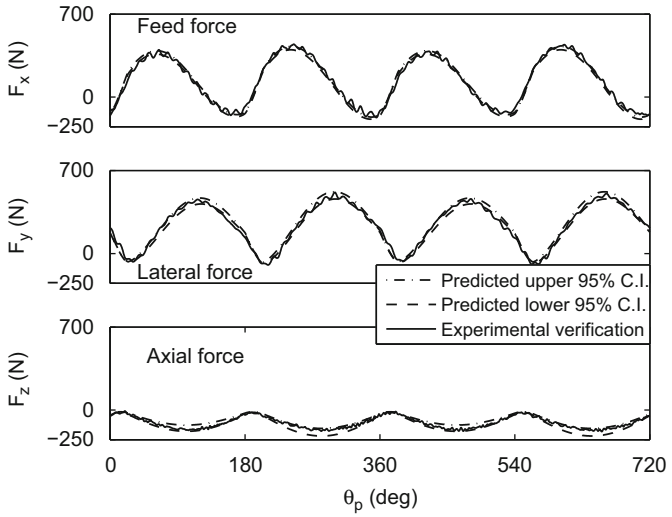

Fig. 12. Predicted vs. experimental force signals: equispaced, 2-fluted, 45° helix cutter; feed 0.100 mm/tooth, 100% radial immersion slotting. Nominal runout 10 μm. Other conditions as in Table 2.

reliably extracted with a low radial immersion experiment. This results in considerable material savings in the cutting coefficient determination experiment, and proves useful when expensive materials are to be machined. This also permits experimental extraction of cutting coefficients for large axial depths of cut on machines in which spindle power limitations may not permit slotting cuts at such depths.

Another advantage of the model was demonstrated which is that the helix angle effects, if any, are automatically taken care of while extracting cutting coefficients. It is not necessary to invoke the fact that cutting coefficients are independent of helix angles, and then use the theoretical expressions for a slotting cut with a zero helix.

An uncertainty analysis has been performed. It has been shown how the expanded uncertainty may be computed for the case where both, the Type A and Type B uncertainties exist. This makes it possible to place 95% confidence intervals on predicted forces for any practical situation. The mathematical structure of the force model permits the analytical derivation of sensitivity coefficients which were used in the uncertainty analysis. The availability of single equations for the entire domain keeps the analytical calculations compact. This is one example of the usefulness of this force model in applications.

The uncertainty analysis was carried out considering the effects of possible correlation between the cutting constants in the plane. This yields tight confidence intervals. If the user so chooses, an abridged method can be used where the correlation is ignored, i.e., the covariances are not considered in calculating the propagation of uncertainties in the cutting constants. Nominal values of cutting constants and their variances can be quickly assessed using single equation regression. The ability to provide a defensible uncertainty statement to accompany cutting force predictions is beneficial in practice. It enables the user of the force model to decide the usefulness of the predictions in any specific application.

One limitation of the model stems from the fact that the geometry of the chip formed should correspond to that postulated here. This geometry is characteristic of chips obtained in the milling of ductile metallic alloys. The authors have experimentally validated the model using an aluminum alloy as outlined in this paper. A version of the model using average cutting coefficients has been validated using a plain carbon steel and an aluminum alloy as detailed in [3].

The mechanism of machining of ductile metallic alloys involves cutting (shearing at interatomic planes) and plowing actions. Shearing is the dominant mode of power consumption in general applications. For micromachining, especially when the order of magnitude of the feed is the same as the edge rounding radius of the sharp cutting edges, the plowing action can consume comparable amounts of power. Plowing is better modeled as being proportional to the length of the cutting edge in contact with the chip. The related lumped parameter coefficients are called edge coefficients, but are ignored in the model presented in this paper. Hence, the model outlined here should not be used directly in micromachining applications, nor for feed rates which are so low as to be of order of magnitude similar to the edge radii of the sharp cutting edges. An augmented version of this model would be necessary. The formulation of the required augmentation is outlined in [3].

Acknowledgements

One of the authors (A.B.) would like to acknowledge the Alumni Fellowship, of the University of Florida, which enabled him to engage in this research. He would also like to thank Scott W.T. Payne and Vadim J. Tymianski for their generous assistance with the experimental work.

Appendix A

A.1. Line segments describing θ_L, θ_T, and b

For the sake of illustration, the line segment describing θ_L is shown below. The variation of θ_L in Type I and Type II cutting is the same as is readily observed by inspection of Fig. 4. The functional relationship between θ_L and θ,[5] is

$$\left.\begin{array}{ll} \theta_L = 0, & 0 \le \theta < \theta_{st} \\ \theta, & \theta_{st} < \theta \le \theta_{ex} \\ \theta_{ex}, & \theta_{ex} \le \theta \le \theta_{ex} + \dfrac{2a\tan\lambda}{D} \\ 0, & \theta_{ex} + \dfrac{2a\tan\lambda}{D} < \theta < 2\pi \end{array}\right\} \quad (65)$$

Expressions for θ_T and b may be similarly obtained.

[5] In the derivations, the subscript, $_p$, is dropped from θ_p for the sake of simplicity.

A.2. Derivation of Fourier coefficients

Fourier coefficients L_0, L_k, M_k, T_0, T_k, R_k, B_0, B_k, and C_k, may be derived by inspection of Fig. 4, writing out the functional relationships valid for the fundamental period, $\theta_p \in [0,2\pi)$, and integrating appropriately using standard Fourier series procedures [11].

As an example, the Fourier coefficients, L_k, is derived below. Other coefficients are derived in a similar manner.

$$L_k = \frac{1}{\pi}\int_0^{2\pi} \theta_L \cos\theta \, d\theta = \frac{1}{\pi}\left[\int_{\theta_{st}}^{\theta_{ex}} \theta \cos\theta \, d\theta + \int_{\theta_{ex}}^{\theta_{ex}+2a\tan\lambda/D} \theta_{ex}\cos\theta \, d\theta\right]$$

Simplification yields Eq. (14).

A.3. Estimation of cutting constants

Following the method of Zellner [26], the multiresponse model for the simultaneous estimation of the cutting constants $\Gamma_{tc,nc}$ and $\Psi_{tc,nc}$ of Eq. (40), may be written as

$$\mathbf{K}_i = \mathbf{H}_i\boldsymbol{\beta}_i + \boldsymbol{\varepsilon}_i \quad i = tc,nc \tag{66}$$

where v is the number of experimental data sets, $\mathbf{K}_i$ is a $v \times 1$ vector of the (logarithms of the) cutting coefficient responses, $\boldsymbol{\beta_i}$ is a 2×1 vector of unknown constant parameters (the cutting constants), $\boldsymbol{\varepsilon_i}$ is a random error vector associated with the i th response, and

$$\mathbf{H}_{tc} = \mathbf{H}_{nc} = [\underset{v\times 1}{\mathbf{1}} \quad \underset{v\times 1}{\ln\bar{\mathbf{h}}_\mathbf{m}}] \tag{67}$$

where $\{\ln\bar{\mathbf{h}}_\mathbf{m}\}$ is the vector of (the logarithms of) the averaged mean chip thickness at which the responses are observed.

In matrix notation, Eq. (66) may be rewritten with $\mathbf{H}$ appearing in block diagonal form

$$\underbrace{\begin{Bmatrix} \underset{v\times 1}{\ln\mathbf{K}_{tc}} \\ \underset{v\times 1}{\ln\mathbf{K}_{nc}} \end{Bmatrix}}_{\mathbf{K}} = \underbrace{\begin{pmatrix} \underset{v\times 2}{\mathbf{H}_{tc}} & \mathbf{0} \\ \mathbf{0} & \underset{v\times 2}{\mathbf{H}_{nc}} \end{pmatrix}}_{\mathbf{H}} \underbrace{\begin{Bmatrix} \Gamma_{tc} \\ \Psi_{tc} \\ \Gamma_{nc} \\ \Psi_{nc} \end{Bmatrix}}_{\boldsymbol{\beta}} + \underbrace{\begin{Bmatrix} \underset{v\times 1}{\boldsymbol{\varepsilon}_{tc}} \\ \underset{v\times 1}{\boldsymbol{\varepsilon}_{nc}} \end{Bmatrix}}_{\boldsymbol{\varepsilon}} \tag{68}$$

Zellner [26] has given an example which shows the method of estimating the multiple response parameters (the two-stage Aitken estimators), and obtaining the variance–covariance matrix (the moment matrix) of these estimators. The example is symbolically reproduced here with suitable changes in notation. Rewriting Eq. (68) in a simplified manner, the system to be estimated is

$$\begin{Bmatrix} K_t \\ K_n \end{Bmatrix} = \begin{pmatrix} H_t & 0 \\ 0 & H_n \end{pmatrix} \begin{Bmatrix} \beta_t \\ \beta_n \end{Bmatrix} + \begin{Bmatrix} \varepsilon_t \\ \varepsilon_n \end{Bmatrix} \tag{69}$$

First, the single-equation least squares estimates are obtained in the usual way. These estimates are

$$\hat{\beta}_t = \begin{Bmatrix} \hat{\beta}_{t0} \\ \hat{\beta}_{t1} \end{Bmatrix} = \begin{Bmatrix} \Gamma_{tc} \\ \Psi_{tc} \end{Bmatrix} \quad \text{and} \quad \hat{\beta}_n = \begin{Bmatrix} \hat{\beta}_{n0} \\ \hat{\beta}_{n1} \end{Bmatrix} = \begin{Bmatrix} \Gamma_{nc} \\ \Psi_{nc} \end{Bmatrix}$$

To obtain the disturbance covariance matrix, it is convenient to write

$$[K_t \; K_n] = [H_t \; H_n] \begin{pmatrix} \hat{\beta}_t & 0 \\ 0 & \hat{\beta}_n \end{pmatrix} + [\hat{u}_t \; \hat{u}_n] \quad \text{or} \quad K = HB + \hat{U}$$

Then

$$\begin{aligned} \hat{U}^T\hat{U} &= (K-HB)^T(K-HB) = K^TK - B^TH^THB \\ &= \begin{pmatrix} K_t^TK_t & K_t^TK_n \\ K_n^TK_t & K_n^TK_n \end{pmatrix} - \begin{pmatrix} \hat{\beta}_t^TH_t^TH_t\hat{\beta}_t & \hat{\beta}_t^TH_t^TH_n\hat{\beta}_n \\ \hat{\beta}_n^TH_n^TH_t\hat{\beta}_t & \hat{\beta}_n^TH_n^TH_n\hat{\beta}_n \end{pmatrix} \\ &= (v-2)\{s_{\mu\mu'}\} \end{aligned}$$

where $s_{\mu\mu'}$ is an estimate of the (unknown) expectation value $\sigma_{\mu\mu'} = E(u_\mu u_{\mu'})$, and $\mu,\mu' = t,n$. This last matrix may be inverted to obtain $(v-2)^{-1}\{s^{\mu\mu'}\}$. Knowing $s^{\mu\mu'}$ enables one to obtain the following symmetric moment matrix of the two-stage Aitken estimators:

$$V(\beta) = \begin{pmatrix} s^{tt}H_t^TH_t & s^{tn}H_t^TH_n \\ s^{nt}H_n^TH_t & s^{nn}H_n^TH_n \end{pmatrix}^{-1} \tag{70}$$

whose diagonal elements are the estimated coefficient estimator variances, and off-diagonal elements are estimated covariances.

The two-stage Aitken coefficient estimates are

$$\beta = V(\beta)\begin{Bmatrix} s^{tt}H_t^TK_t + s^{tn}H_t^TK_n \\ s^{nt}H_n^TK_t + s^{nn}H_n^TK_n \end{Bmatrix} \tag{71}$$

For the experiments analyzed in this paper, $H_t = H_n$, and the two-stage Aitken estimators are the same as the single equation least squares estimators, but the variance–covariance matrix, $V(\beta)$, is not diagonal, i.e., the covariances are non-zero.

References

[1] F. Abrari, M.A. Elbestawi, Closed form formulation of cutting forces for ball and flat end mills, International Journal of Machine Tools and Manufacture 37 (1) (1997) 17–27.
[2] Y. Altintas, A. Spence, End milling force algorithms for CAD systems, Annals of the CIRP 40 (1991) 31–34.
[3] A. Bhattacharyya, Predictive force modeling of peripheral milling, Ph.D. Dissertation, University of Florida, 2008.
[4] R. Cadille, Manufacturer's certificate, Kistler Instrument Corp., Amherst, NY, 2008.
[5] R. Dieck, Measurement uncertainty models, ISA Transactions 36 (1) (1997) 29–35.
[6] K.F. Ehman, S.G. Kapoor, R.E. DeVor, I. Lazoglu, Machining process modeling: a review, Journal of Manufacturing Science and Engineering 119 (1997) 655–663.
[7] S. Engin, Y. Altintas, Mechanics and dynamics of general milling cutters. Part I: helical end mills, International Journal of Machine Tools and Manufacture 41 (15) (2001) 2195–2212.
[8] S. Jayaram, S.G. Kapoor, R.E. DeVor, Estimation of the specific cutting pressures for mechanistic cutting force models, International Journal of Machine Tools and manufacture 41 (2001) 265–281.
[9] W.A. Kline, R.E. DeVor, The effect of runout on cutting geometry and forces in endmilling, International Journal of Machine Tool Design and Research 23 (2–3) (1983) 123–140.
[10] J.H. Ko, W.-S. Yun, D.-W. Cho, K.F. Ehman, Development of a virtual machining system, part 1: approximation of the size effect for cutting force prediction, International Journal of Machine Tools and Manufacture 42 (2002) 1595–1605.
[11] E. Kreyszig, Advanced Engineering Mathematics, ninth ed., John Wiley & Sons, Inc, Hoboken, NJ, 2006.
[12] M.H. Kurdi, Robust multicriteria optimization of surface location error and material removal rate in high speed milling under uncertainty, Ph.D. Dissertation, University of Florida, 2005.
[13] B. Mann, B. Edes, S. Easley, K. Young, K. Ma, Chatter vibration and surface location error prediction for helical end mills, International Journal of Machine Tools and Manufacture 48 (3–4) (2008) 350–361.
[14] M. Martellotti, An analysis of the milling process, Transactions of the ASME, Journal of Engineering for Industry 63 (1941) 667–700.
[15] A. Sabberwal, Chip section and cutting force during the milling operation, CIRP Annals 10 (1961) 197–203.
[16] C. Salomon, Die Fräsarheit, Werkstattstechnik 20 (1926) 469–474.
[17] N. Sawin, Theory of milling cutters, Mechanical Engineering 48 (1926) 1203–1209.
[18] T. Schmitz, B. Mann, Closed-form solutions for surface location error in milling, International Journal of Machine Tools and Manufacture 46 (12–13) (2006) 1369–1377.
[19] Y.C. Shin, A.J. Waters, A new procedure to determine instantaneous cutting force coefficients for machining force prediction, International Journal of Machine Tools and Manufacture 37 (9) (1997) 1337–1351.
[20] B.N. Taylor, C.E. Kuyatt, NIST Technical Note 1297, 1994 edition: Guidelines for evaluating and expressing the uncertainty of NIST measurement results, United States Department of Commerce Technology Administration, National Institute of Standards and Technology, Gaithersburg, MD, 1994.
[21] J. Tlusty, Manufacturing Processes and Equipment, Prentice-Hall, Upper Saddle River, NJ, 2000.
[22] J. Tlusty, P. MacNeil, Dynamics of cutting forces in end milling, Annals of the CIRP 24 (1) (1975) 21–25.
[23] D. Turzeniecka, Errors in the evaluation of the coverage factor as a criterion of applications of approximate methods of evaluation of expanded uncertainty, Measurement 27 (2000) 223–229.

[24] L. Xu, J. Schueller, J. Tlusty, A simplified solution for the depth of cut in multi-path ball end milling, Machining Science and Technology 2 (1) (1998) 57–75.
[25] L. Yang, R.E. DeVor, S.G. Kapoor, Analysis of force shape characteristics and detection of depth-of-cut variations in end milling, Transactions of the ASME, Journal of Manufacturing Science and Engineering 127 (2005) 454–462.
[26] A. Zellner, An efficient method for estimating seemingly unrelated regressions and tests for aggregation bias, Journal of the American Statistical Association 57 (298) (1962) 348–368.